Electromechanical Energy Conversion Systems (EECS)
Niroo Research Institute (NRI)
Vol. 4, No. 1, Spring 2025, pp. 1-16
DOI: 10.30503/EECS.2025.475476.1060
Review Article

A Survey on Brushless DC Motors: Drive Circuits, Control Schemes, and Rotor Position Identification Methods

Mahdi Abolghasemi[1*], Aghil Ghaheri[1], Ali Harooni[1], Seyyed Ebrahim Afjei[1]

Abstract

The drive circuits play an essential role in the operation of Brushless DC motors. These circuits facilitate effective commutation and control, directly influencing motor performance and efficiency. Various drive circuit configurations are analyzed, highlighting their impact on torque delivery and overall system responsiveness. The significance of selecting appropriate drive circuit designs tailored to specific applications, enhancing reliability and functionality is addressed. In addition, various common switching methodologies, known as control methods to manipulate the torque and rotational velocity characteristics are discussed. This study investigates the influence of rotor position identification techniques on the performance of Brushless DC motors. Accurate rotor position detection is essential for effective commutation, directly impacting torque generation and overall efficiency. This research compares various methods, including sensor-based and sensorless approaches, highlighting their respective advantages and limitations. The findings reveal that sensorless techniques, while cost-effective, may compromise precision under variable load conditions. In contrast, sensor-based methods provide enhanced accuracy but at the expense of increased complexity and cost. The study further explores the implications of these techniques on the operational characteristics of Brushless DC motors, particularly in applications requiring high reliability and performance. The discussions underscore the necessity for selecting appropriate rotor position identification methods tailored to specific application requirements, thereby advancing the understanding of Brushless DC motor technology.

Keywords: Brushless DC motor, Control, Drive system, Inverter, Sensorless.

Received Date: 2024-08-27; Revised Date: 2024-12-28; Accepted Date: 2025-01-08 .

1. INTRODUCTION

Brushless DC (BLDC) motors feature a rotor with permanent magnets and a stator with wound coils, eliminating brushes for enhanced efficiency. Their compact design, high torque-to-weight ratio, and durability make them pivotal in applications ranging from electric vehicles to robotics, driving innovation in energy-efficient technologies and precision engineering. Thus, this kind of motor benefits from a simple structure, high efficiency, long life span, high torque density, precise controllability, fast dynamic response, and low acoustic noise. Nevertheless, BLDC motors suffer from higher construction costs, more difficult maintenance, and high phase current during the start period, compared with some of the conventional electric motors in the industry [1].

In BLDC motors, the design and implementation of drive and control circuits are essential, significantly increasing costs. Although the motor has a simple structure, its drive and control circuits are complex, complicating troubleshooting. During startup, the phase currents can surge to over ten times the steady-state current, raising coil temperatures and similarly affecting torque characteristics. Designers must account for these factors in their designs. To have a better insight into the BLDC motors, the most proper candidates for Electric vehicle application are compared in Table 1, proving the superiority of the BLDC motors.

[1] *Department of Electrical Engineering, Shahid Beheshti University, Tehran, Iran*
**Corresponding author, Email: m.abolghasemi@hotmail.com*

TABLE. 1. Various electric motors comparison for electric vehicles application [1]

	DC Motor	Induction Motor	BLDC Motor	Switched Reluctance Motor
Power Density	Low	Medium	High	Very high
Maximum Efficiency (%)	< 90	90 - 95	95 – 97	< 90
Rated Load Efficiency (%)	80 – 87	90 – 92	85 – 97	< 90
Controllability	Simple	Very hard	Hard	Very hard
Reliability	Medium	High	Very high	high
Thermal Dissipation	Low	Low	Good	Good
Volume	Large	Medium	Small	Small
Weight	Heavy	Medium	Light	Light
Performance at High Speeds	Weak	Excellent	Good	Excellent
Cost ($/kW)	10	8 – 10	10 – 15	6 – 10
Controller Cost	Low	High	High	Medium

The BLDC motors require drive and control systems to function effectively across all four operational quadrants. Various circuits, each with distinct characteristics, are employed to energize the motor coils. Accurate rotor position detection is crucial for precise motor operation, achievable through either the sensor-based or the sensorless techniques. This paper presents an overview of the most prominent drive, control, and rotor position detection circuits and methodologies. It evaluates the advantages and disadvantages of each approach, providing valuable insights into the available options for electric motor designers. By elucidating these technologies, the paper aims to enhance understanding and facilitate informed decision-making in the design and implementation of the BLDC motor systems, ultimately contributing to advancements in efficiency and performance in various applications.

2. WELL-KNOWN DRIVE CIRCUITS

Prior to introducing the drive circuits, it is necessary to have a glimpse of the operating regions of the BLDC motors. The performance of a motor is defined by the sign of speed and torque across four operational regions. Depending on their architecture, existing drive systems and control methods can be implemented in two or four operational regions. The specifics of these regions are outlined below:

I. First region: Normal rotation.
II. Second region: Reverse braking.
III. Third region: Reverse rotation.
IV. Fourth region: Normal braking.

2.1. Half-Wave Inverters

Half-wave inverters utilize fewer power switches compared to their full-wave counterparts, which can lead to reduced efficiency. However, their advantages make them suitable for specific applications. These inverters are more compact and cost-effective, resulting in smaller drive systems and cooling requirements. Given the prevalence of BLDC motors in everyday devices, economic feasibility is crucial for their adoption. Consequently, half-wave inverters are ideal for less sensitive applications, such as cleaning appliances, HVAC systems, dryers, and electric wheelchairs. In some contexts, these inverters are also referred to as half-pole inverters. By balancing cost and performance, half-wave inverters provide a viable solution for various consumer products, ensuring they meet economic criteria while maintaining functionality [2].

2.2. Split-Source Half-Wave Inverters

The circuit layout and waveforms of this inverter, depicted in Fig. 1 and 2, respectively, enable the four-quadrant operation of the BLDC motor. To illustrate its functioning, let's consider Phase *A* operation in the first quadrant. At 30 degrees back-EMF, the switch T_1 closes, directly applying voltage V_S to Phase *A*. If the phase current exceeds the

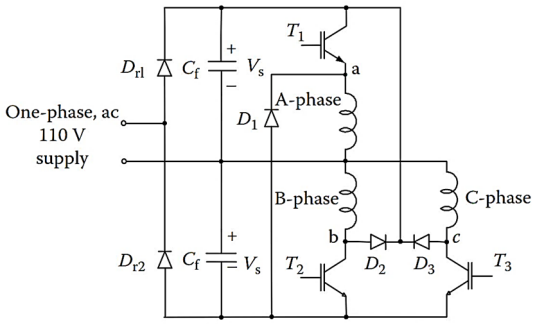

Fig. 1. Split-source half-wave inverter structure [2]

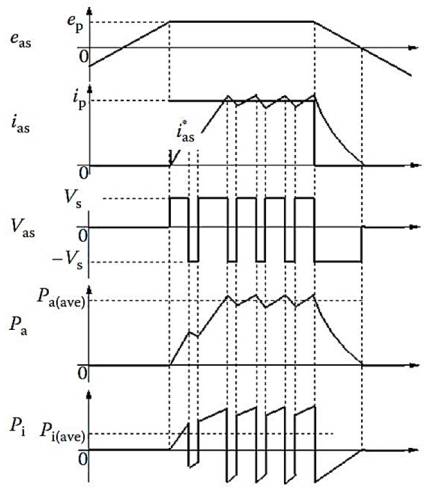

Fig. 2. Split-source half-wave inverter waveforms [2]

TABLE. 2. Operational modes of split-source half-wave inverter [2]

Mode	T_1	T_2	D_1	D_2	i_{as}	i_{bs}	V_{as}	V_{bs}
1	On	Off	Off	Off	>0	0	V_s	0
2	Off	Off	On	Off	>0	0	- V_s	0
3	Off	On	On	Off	>0	>0	- V_s	V_s
4	Off	Off	On	On	>0	>0	- V_s	- V_s

reference value, the T_1 opens via the PWM or hysteresis switching techniques. With the T_1 open, the phase current freewheels through the D_1, the Phase A, and the DC link capacitor, applying the $-V_S$ to the phase. This negative voltage transfers energy from the motor to the DC link, reducing the current value. Thus, the current is controlled by a single switch. The average power from the DC source to the motor is positive, indicating motor operation.

To brake and stop a motor operating in Region 1, negative torque must be applied, effectively transitioning it to Region 4. Since the current cannot be negative, the only viable approach is to delay braking until the back-EMF voltage becomes negative. It is important to note that once this occurs, a waiting period of approximately 30 degrees is necessary before the current becomes negative, at which point switching can occur.

For operating a BLDC motor in Region 3, it suffices to change the phase sequence from *ABC* to *ACB*, altering the motor's rotational direction. The operational states of the inverter for driving the BLDC motor with phases *A* and *B* are detailed in Table 2, which is applicable to any phase pair.

A key distinction between a full-bridge inverter and a split-source inverter lies in the latter's application of positive or negative voltage while the current is still flowing. This design drawback leads to continuous energy circulation within the circuit, resulting in increased losses and reduced efficiency. Additionally, it contributes to higher torque ripple, which can cause increased acoustic noise from the motor. The advantages and disadvantages of this structure are summarized as follows.

Advantages:

- ✓ It needs only one diode and one switch for each phase leading to lower cost compared with its full-wave (full-bridge) counterpart.
- ✓ Reduced gate signal generator and logical control circuits.
- ✓ Applicable in all four quadrants.
- ✓ It can start the motor with only a single switch, a fascinating feature as any phase faces failure.
- ✓ Lower conduction loss.
- ✓ It enables the operator to derive back-EMF by monitoring the switch voltage when it is open, appropriate for sensorless-based control systems.

Disadvantages:

- × Unable to utilize the full capacity of the motor due to its half-wave nature.
- × There is a need for an additional DC link capacitor.
- × Increased self-inductance leading to the motor electrical time constant and dynamic response increment.
- × Torque ripple frequency increment.

2.3. C-Dump Half-Wave Inverters

A significant drawback of the split-source half-wave inverter is its reliance on a single switch per phase, which limits the utilization of only half the maximum DC voltage. This issue can be mitigated by employing an inverter design that incorporates more than one switch per phase, ideally between one and two. The C-Dump configuration exemplifies this approach, featuring *(n+1)* power switches for an n-phase motor; for instance, a three-phase motor would utilize four switches. The C-Dump inverter structure and key waveforms are illustrated in Fig. 3 and 4. This inverter is capable of operating across all four performance regions of a BLDC motor. It comprises four transistors and four power diodes, with one transistor and diode allocated for each phase, plus an additional pair for energy recovery through capacitor C_0 [3].

Assuming a clockwise rotation for the motor, this direction is considered positive, resulting in a phase sequence of *ABC*. Similar to a split-source inverter, when the back EMF voltage reaches a constant value at 30 degrees, switch T_a closes, applying voltage V_s to phase *A*. If the phase current exceeds the reference current, switch *Ta* opens, directing phase *A* current through diode *Da* to the energy recovery capacitor C_0. While switch *Ta* is open, a negative voltage of E-V_{dc} is applied to phase *A*, leading to a reduction in phase current. In this state, both the average air gap power and the positive input power indicate operation within the first quadrant of the BLDC motor's performance. To reverse the motor's direction and operate in the third quadrant, it is sufficient to change the phase sequence from *ABC* to *ACB*.

When energy flows from a load to a motor, the motor operates in generator mode, characterized by opposing signs of speed and torque. Unlike full-wave inverters, a C-Dump inverter cannot generate a negative current to produce negative torque. Consequently, the only option is to delay motor braking until the back EMF voltage becomes negative. It is crucial to wait for 30 degrees after

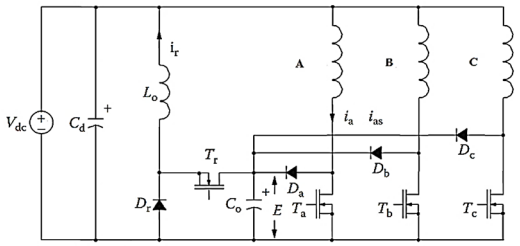

Fig. 3. Three-phase C-dump half-wave inverter structure [2]

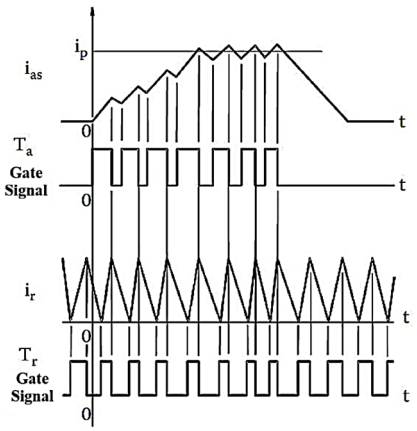

Fig. 4. Three-phase c-dump half-wave inverter waveforms [2]

the back EMF voltage turns negative before stopping the motor, as the current will then be negative, necessitating a switching action. During this phase, both the average power and input power are negative, indicating energy transfer from the motor to the energy recovery capacitor, C_0. This process is essential for effective energy management in regenerative braking systems, allowing for the recovery of energy during deceleration and enhancing overall system efficiency.

The C-Dump inverter has lower losses than the full-wave inverter; however, it has a critical drawback: high current ripple. This excessive ripple significantly increases torque ripple in the BLDC motor.

2.4. Buck-Type Converter-based Inverters

The variable DC source inverter is a step-down converter derived from the conventional half-wave inverter combined with a buck converter. This inverter allows for easy adjustment of the input DC voltage and incorporates the advantages of both split-source and C-Dump inverters. It consists of four power switches and four power diodes, structured in two levels: the first being a buck converter and the second a simple half-wave inverter. Its configuration is illustrated in Fig. 5. The operation of this inverter will be analyzed within the first and fourth quadrants of BLDC motor utilization.

Assuming the motor rotates clockwise, which is considered the positive direction, the phase sequence is *ABC*. The motor operation begins when a constant positive voltage is applied to the inverter for 120 degrees. After switch *T1* in phase *A* closes, current flows through it. When *T1* turns off, current flows through diode *D1*, the DC voltage source, and capacitor *C*, and the voltage at the inverter input becomes $V_i - V_{dc}$. To reverse the motor direction and operate it in the third quadrant, simply change the phase sequence from *ABC* to *ACB*. In this case, the motor operates in the third quadrant.

When energy flows from the load back to the source, the motor operates in generator mode with negative torque. To achieve this negative torque, switch *T1* must be closed when the back EMF voltage is a stable negative value. Based on the rotor position and torque sign, the appropriate power switch is identified, allowing current to flow in the corresponding phase. In previous inverters, phase current was regulated using hysteresis control or PWM, which influenced the switching pattern of the inverter's power switches. This inverter also allows phase current control through adjustments to the DC input voltage, providing designers and operators with greater flexibility in implementing various control strategies.

The advantages of buck-type converter-based inverters are as follows:

- ✓ It only needs four diodes and four power switches to operate in all four quadrants.
- ✓ Reduced gate signal generator circuits.
- ✓ May be operated when one of the switches fails.
- ✓ Lower switching loss.
- ✓ Lower switches voltage stress.
- ✓ Lower current ripple.

The drawbacks of this BLDC motor drive structure are similar to those of all half-wave inverters. These include underutilization of the motor's full capacity, larger time constants, and lower efficiency. Additionally, the presence of an extra voltage level slightly increases switching losses. It's worth noting that this structure can also be implemented using a boost converter, but due to the similarity in underlying principles, it is not discussed

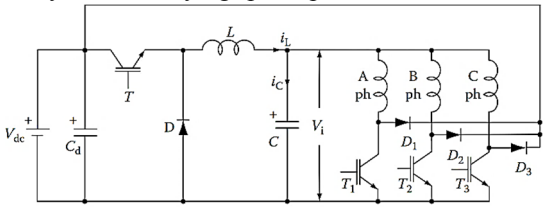

Fig. 5. Buck-type converter-based inverter structure [2]

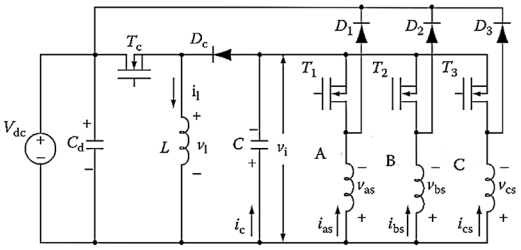

Fig. 6. Buck-boost-type converter-based inverter structure [2]

TABLE. 3. Operational modes of buck-type converter-based inverter [2]

Mode	T_C	D_C	i_1	T_1	D_1	i_{as}
I	On	Off	>0	On	Off	>0
II	Off	On	>0	On	Off	>0
III	On	Off	>0	Off	On	>0
IV	Off	On	>0	Off	On	>0
V	Off	Off	0	On	Off	>0
VI	On	Off	>0	Off	Off	0
VII	Off	Off	0	Off	On	>0
VIII	Off	On	>0	Off	Off	0
IX	off	Off	0	Off	Off	0

further. The calculation of inductor and capacitor values for the buck stage of this inverter is addressed in [4].

2.5. Buck-Boost-Type Converter-based Inverters

The distinction between variable DC source inverters of the buck-boost type and buck type lies primarily in their operational levels. The buck-boost inverter employs a buck-boost converter instead of a buck converter. As illustrated in Fig. 5, the buck-type inverter allows the input DC voltage to range from 0% to 100% of the variable DC supply, whereas the buck-boost inverter can vary from 0% to 200%.

At low motor speeds, minimal DC supply voltage is necessary due to the reduced back-EMF. Consequently, the duty cycle of the buck-boost converter is configured to function as a buck converter, thereby minimizing current ripple and torque ripple. Conversely, at high speeds, traditional systems restrict back-EMF to 60%-80% of the DC supply voltage. However, the buck-boost configuration enables back-EMF to exceed this threshold, allowing for broader speed control.

Various operational modes can be achieved through different combinations of switch and diode states, as summarized in Table 3, which assumes phase A is active while other phase diodes are inactive. The first four modes represent distinct conduction states without circulating paths through the diodes, while the subsequent five modes involve current flow through the diode of the same phase. Understanding these modes is crucial for analyzing motor performance variables, particularly focusing on the first mode in state space, where state variables include inductor current, input DC voltage, and phase currents. The advantages and disadvantages of this type of inverter are as follows [5, 6].

Advantages:

- ✓ The structure requires only four transistors and four diodes to operate the BLDC motor across all four quadrants.
- ✓ It allows for independent control of phase currents.
- ✓ The commutation voltage is zero and equal to the negative of the DC supply voltage.
- ✓ Since the phase switches operate similarly, circuit complexity is reduced.
- ✓ The DC supply voltage can vary from zero to twice the nominal voltage (V_{dc}), enhancing phase current response, decreasing electrical time constants, and minimizing switching losses.
- ✓ Reduced current ripple due to low DC voltage at low speeds leads to lower torque ripple and, consequently, less motor noise.
- ✓ At high speeds, unlike previous drive systems where back-EMF voltage is limited to 60-80% of the DC supply, this structure employs a buck-boost converter, allowing for higher back-EMF and broader speed control, thus increasing motor output power.

Disadvantages:

- × The motor's full capacity is not utilized.
- × The nominal volt-ampere rating of the switches is high.
- × The additional converter reduces overall system efficiency compared to configurations without it.
- × Discontinuous currents in capacitors (C and C_d) increase the current ripple in these components.
- × Coordination between the first and second levels of inverter control is necessary.

2.6. Six-Switch Full-Wave Inverters

The schematic diagram of the six-switch full-wave inverter is depicted in Fig. 7. This configuration operates in two primary modes: two-phase conduction and three-phase conduction. As previously noted, Permanent Magnet Synchronous Motors (PMSMs) utilize three-phase conduction, while the BLDC motors rely on two-phase conduction, where only two phases carry current at any given moment. The switching pattern of this inverter is determined by the rotor's position, with two switches

active at all times while the others remain off. If both switches are from the same leg of the bridge, no current flows through any phase, and simultaneous activation of both switches in one branch results in a short circuit. Therefore, these considerations must be addressed during the control circuit design. A complete cycle consists of six intervals of 60 degrees, with switches toggling at each interval. The primary advantage of this structure is its minimal output current and voltage ripple, making it the most widely used configuration in the industry, also referred to as a six-stage inverter [7].

2.7. H-Bridge Full-Wave Inverters

The H-bridge inverter structure, illustrated in Fig. 8, is a single-phase configuration comprising four power switches. To adapt this design for a three-phase motor, three single-phase H-bridge inverters are required, resulting in a total of twelve power switches, which significantly increases switching losses. Despite its simplicity, the H-bridge allows for independent control of each phase's current, a crucial feature for handling asymmetric motors and unbalanced loads. This capability enhances the range of control strategies available to designers and operators. The switches operate in a cross-coupled manner, meaning that switches *(T_1, T_4)* and *(T_2, T_3)* are activated and deactivated simultaneously to prevent short circuits. Additionally, a dead time must be incorporated between switch transitions to avoid momentary short circuits, which are longer in this structure compared to others, representing a disadvantage of the H-bridge inverter. Consequently, its use in three-phase motors is generally not recommended [8,9].

2.8. Four-Switch Full-Wave Inverters

The structure of the four-switch inverter, illustrated in Fig. 9, closely resembles that of the six-switch inverter. By replacing the power switches in one branch of the six-switch inverter with two capacitors, a four-switch configuration is achieved. This reduction in the number of power switches leads to decreased switching losses, resulting in higher efficiency compared to the six-switch design. However, a notable drawback is the increased torque ripple in the four-switch inverter. As depicted, only two phases of this inverter can be controlled, limiting control over the phase connected to the capacitor branch. Additionally, conventional PWM techniques cannot be employed for switching due to the asymmetrical nature of the voltage waveforms caused by the capacitor connection. Consequently, the space vector pulse width modulation (SVPWM) must be utilized, although it is not the only available method for this configuration [10-13].

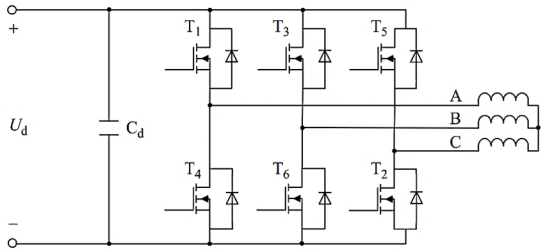

Fig. 7. Three-phase six-switch full-wave inverter structure [2]

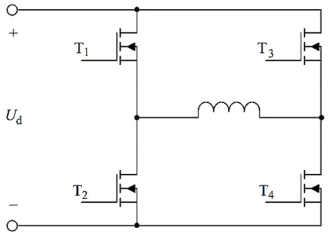

Fig. 8. Single-phase H-bridge full-wave inverter structure [2]

3. COMMON CONTROL SCHEMES

Switching methods are inherently control techniques. Common methods for controlling the BLDC motors include the PWM, the Pulse Amplitude Modulation (PAM), the SVPWM, and the hysteresis control. Designers often prefer not to use SVPWM due to its complexity, which can complicate analysis and implementation. This complexity leads many engineers to favor adaptive control methods instead [14]. Consequently, this paper will focus on examining the PWM, the PAM, the PAM/PWM, and the hysteresis methods.

3.1. PWM Technique

In this method, two signals, referred to as the reference signal and the carrier signal, are compared. The reference signal represents the desired output for the designer and operator, while the controller aims to achieve this output. The carrier signal is a saw-tooth waveform with an amplitude greater than that of the reference signal. By comparing these two signals, the voltage applied to each power switch, and consequently the switching behavior of each switch, is determined. In fixed-frequency PWM, the average output current remains constant, allowing for the reduction of output current harmonics through the design of a simple filter.

The PWM methods are categorized as bipolar PWM and unipolar PWM. The bipolar PWM is often referred to as the H-PWM-L-PWM in various references. The unipolar PWM is further categorized into five types: ON-PWM, PWM-ON, PWM-ON-PWM, H-PWM-L-ON, and H-ON-

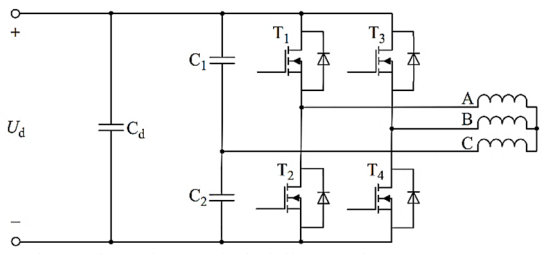

Fig. 9. Three-phase four-switch full-wave inverter structure [2]

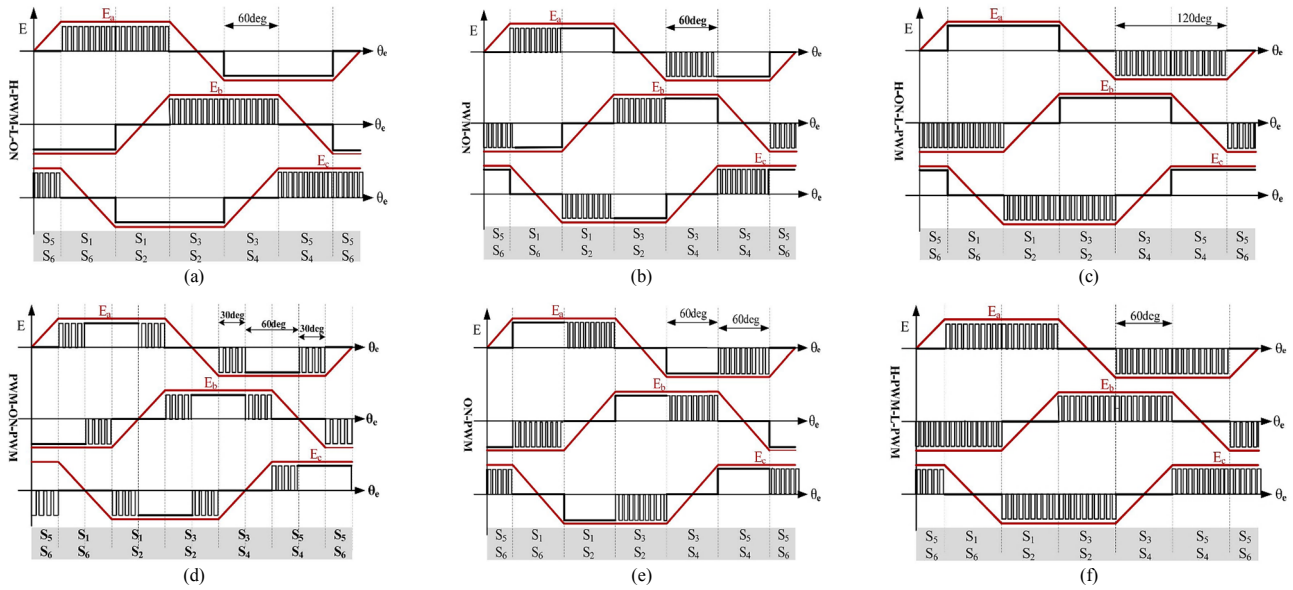

Fig. 10. Trigger signals of various PWM techniques (a) H-PWM-L-PWM (b) PWM-ON (c) H-ON-L-PWM (d) PWM-ON-PWM (e) ON-PWM (f) H-PWM-L-PWM [15]

L-PWM [15]. The triggering signals for these methods are depicted in Fig. 10.

In the H-PWM-L-PWM method, gate signals are applied to both the upper and lower switches using PWM techniques, resulting in switching losses that are twice as high as those in other PWM methods. This approach causes the output voltage to fluctuate between U_d and $-U_d$, imposing greater electrical stress on the power switches. Consequently, switches capable of withstanding higher reverse voltages must be employed. Additionally, this method significantly increases circuit temperature, necessitating a larger heatsink. It also produces more harmonics compared to the unipolar method [16,17]. Nevertheless, the simplicity and cost-effectiveness of developing a control circuit based on this approach make it an attractive option [15].

In the H-PWM-L-ON method, the gate signal is applied to the upper bridge switch using PWM, while the lower bridge switch receives a continuous and constant gate signal during the corresponding period. The gate signals for the switches in the H-ON-L-PWM method are exactly the opposite of the H-PWM-L-ON method.

The PWM-ON and the ON-PWM methods, introduced in [18,19], have identical trigger signals in the 0 to 60-degree range. The H-PWM-L-ON and the ON-PWM have the same gate signals in the 60 to 120-degree range. In the H-PWM-L-ON and the H-ON-L-PWM methods, heat distribution is not uniform, making heatsink selection more challenging. In contrast, the PWM-ON and the ON-PWM methods have a nearly uniform heat distribution, allowing for smaller and more cost-effective heatsinks compared to other methods [16,17].

The PWM-ON and the ON-PWM methods reduce commutation-induced current ripple, while the majority of ripple stems from freewheeling diode currents in inactive phases. The PWM-ON-PWM technique, presented in [19,20], significantly mitigates current and torque ripple by applying PWM signals during the first and last 30 degrees of commutation, virtually eliminating freewheeling diode currents.

Comparing the PWM methods in suppressing freewheeling diode current ripple, ranks them from best to worst:

1. PWM-ON-PWM
2. PWM-ON
3. ON-PWM
4. H-PWM-L-ON
5. H-ON-L-PWM
6. H-PWM-L-PWM

This order also reflects their performance in terms of torque ripple and electromagnetic interference.

3.2. PAM Technique

The PWM method generates significant harmonics, which notably increase losses at high speeds and reduce the system's power factor [22]. At elevated speeds, two or three PWM pulses occur within a 60-degree interval, insufficient for effective speed control, leading to a considerable rise in speed ripple. This increased ripple also contributes to greater vibration and acoustic noise in the motor [22-24].

To mitigate these issues, the PAM method is employed, which results in substantially lower switching losses compared with the PWM. The PAM produces a continuous signal throughout the entire commutation range, making it highly effective for high-speed BLDC motors. In this approach, a continuous signal of logical magnitude is applied to each power switch during its conduction period, adjusting the input voltage based on the desired motor

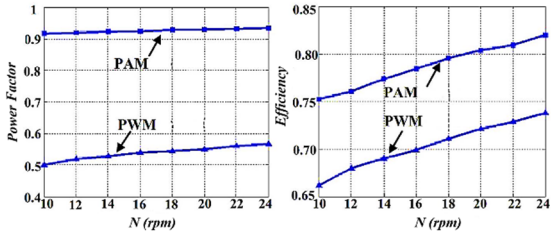

Fig. 11. Comparison of BLDC motor efficiency and power factor with PWM and PAM control techniques [22]

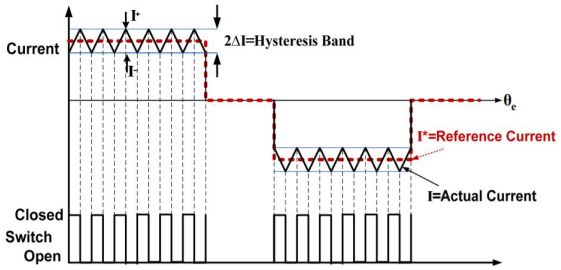

Fig. 12. Current waveform in hysteresis control technique [15]

speed. Many sources utilize a variable DC source three-phase six-switch inverter for input voltage control. However, this structure has the drawback of requiring a large inductor at high voltages, which occupies considerable space and increases electromagnetic compatibility (EMC) issues. Therefore, a controlled rectifier is used for input voltage regulation.

The PAM method does have its drawbacks. To prevent destructive current during motor startup, the input DC voltage must be significantly reduced, which is often impractical. Additionally, this approach considerably diminishes the motor's response speed and acceleration. Fig. 11 compares the efficiency and power factor of a BLDC motor using the PWM and the PAM methods. As illustrated, the PAM method demonstrates significantly better efficiency and power factor.

3.3. PAM/PWM Technique

As discussed before, both the PWM and the PAM methods have their respective advantages and disadvantages. The PAM excels in high-speed applications but performs poorly at low speeds, particularly during startup. In contrast, the PWM demonstrates excellent performance during startup but can induce significant speed ripple at high speeds. Consequently, researchers have combined these two methods to develop the PAM/PWM approach. In this method, the motor is initially started using the PWM, and once the speed exceeds a certain threshold, the central processor switches to the PAM for speed control. This hybrid approach is particularly effective for BLDC motors, which are predominantly utilized in high-speed applications.

3.4. Hysteresis Current Control Technique

As illustrated in Fig. 12, this method maintains the current within a specified range by continuously switching the power switch on and off. When the current exceeds the upper limit of the designated range, the corresponding phase connections are configured to the power supply such that the terminal voltage equals $-U_d$, resulting in a reduction of current. Conversely, if the current falls below the lower limit, the phase connections are adjusted to achieve a terminal voltage of U_d, which increases the current. In BLDC motors, the back-EMF and the current flowing through the motor are proportional to the speed and the difference between the supply voltage and the back-EMF. Consequently, both the current and switching frequency decrease with increasing speed and increase with decreasing speed. However, at low speeds, increasing the hysteresis range can reduce the switching frequency, although this leads to greater torque ripple. Adjusting the hysteresis range alters the inductance through which the current flows and the voltage applied to the motor by the inverter.

Hysteresis control is implemented in the industry in both analog and digital forms. In the analog approach, the instantaneous current is continuously compared with the hysteresis band. Conversely, the digital method involves discrete comparisons of instantaneous current and the hysteresis band. Consequently, the measured current must be converted to digital form using an Analog-to-Digital Converter (ADC), allowing for digital comparison. In this context, the current information is updated based on the ADC's sampling frequency. In digital systems, a lower sampling frequency results in a longer sampling period, which can lead to greater increases in current. Therefore, determining the minimum sampling frequency is crucial for effective hysteresis control in digital controllers.

The hysteresis current control method has a significant drawback compared with PWM techniques. In hysteresis control, the frequency of current variations is variable, making the design of suitable filters for harmonic suppression quite complex. Consequently, this method is typically employed for controlling the BLDC motors only under conditions of minimal load and speed fluctuations. In some references, the hysteresis controller is referred to as a bang-bang controller [15].

3.5. Direct Torque Control Technique

In Direct Torque Control (DTC), both the stator flux and electromagnetic torque can be controlled directly [25,26]. By selecting the appropriate inverter switching state, the discrepancies between the actual and reference torque and magnetic flux can be improved within a hysteresis band, achieving high efficiency and rapid response. Accurate torque estimation is crucial in the DTC. For a trapezoidal back-EMF BLDC motor, the electromagnetic torque in the stationary reference frame is calculated using the following relationship, regardless of whether it is a two-phase or three-phase operation [15]:

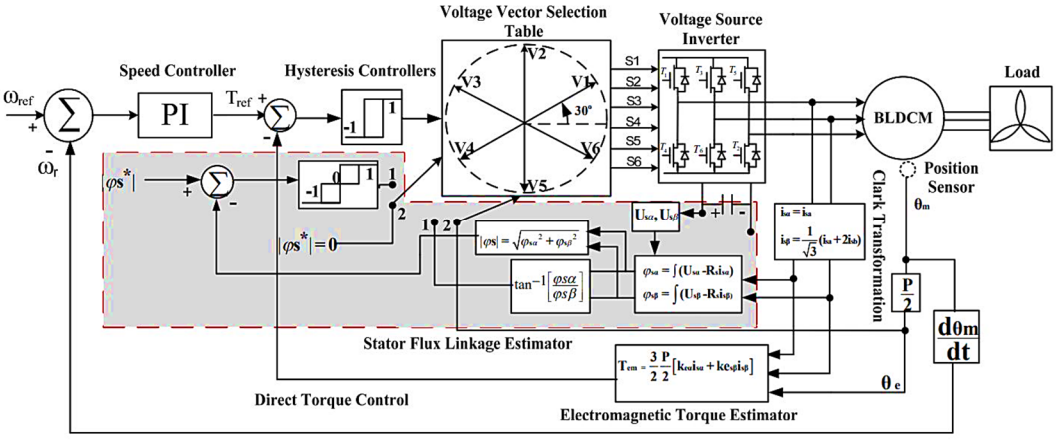

Fig. 13. The direct torque control method block diagram for the BLDC motor [15]

$$T_{em} = \frac{3}{2}\frac{P}{2}\left[\frac{d\psi_{r\alpha}}{dt} i_{s\alpha} + \frac{d\psi_{r\beta}}{dt} i_{s\beta}\right] = \frac{3}{2}\frac{P}{2}\frac{1}{\omega_e}\left[e_\alpha i_{s\alpha} + e_\beta i_{s\beta}\right] = \frac{3}{2}\frac{P}{2}\left[k_{\alpha(\theta_e)} i_{s\alpha} + k_{\beta(\theta_e)} i_{s\beta}\right] \quad (1)$$

Since the final term (1) shows that rotor speed has no influence on electromagnetic torque, this method can accurately estimate torque at zero and near-zero speeds. Therefore, using this expression in motor control is advantageous. The stator flux linkage vector in the $\alpha\beta$ axis is as follows:

$$\varphi_{s\alpha} = \int\left(U_{s\alpha} - R_s i_{s\alpha}\right)dt \ , \ \varphi_{s\beta} = \int\left(U_{s\beta} - R_s i_{s\beta}\right)dt \quad (2)$$

Stator linkage flux angular position may be calculated using the below relations:

$$\varphi = \sqrt{\varphi_{s\alpha}^2 + \varphi_{s\beta}^2} \ , \ \theta = \text{Arctan}\frac{\varphi_{s\alpha}}{\varphi_{s\beta}} \quad (3)$$

The rotor linkage flux may be obtained as follows:

$$\varphi_{r\alpha} = \varphi_{s\alpha} - L_s i_{s\alpha} \ , \ \varphi_{r\beta} = \varphi_{s\beta} - L_s i_{s\beta} \quad (4)$$

The block diagram of the DTC method is depicted in Fig. 13. This diagram comprises four main components: the speed controller, the torque and flux predictor, the flux and torque comparators, and the switching logic processor. The torque and flux predictor is responsible for estimating the actual stator flux, the generated torque, and the magnetic flux position. The comparators include a hysteresis control block that compares the actual flux and torque values with their reference counterparts. The speed controller operates as a PI controller, which adjusts the speed based on rotor position signals compared to a reference speed [15].

According to Table 4, the inverter's switching pattern correlates with the stator's torque and flux linkage. Since only two phases of the three-phase BLDC motor coils are active every 60 degrees, a non-zero voltage space vector is applied to adjust the torque when the actual stator flux deviates from its reference. When the actual flux is less or more than the reference, a non-zero voltage vector is utilized accordingly. Notably, in the DTC method, the magnetic flux controller can be omitted in regions where torque remains constant, as detailed in [17]:

1. Since the back-EMF in the constant torque region is less than half of the DC supply voltage, the magnetic flux in the stator remains nearly constant, eliminating the need for flux control.
2. In two-phase conduction, torque fluctuations occur at the boundaries between commutation intervals, and these fluctuations are entirely unpredictable, influenced by various factors such as sampling time, DC supply voltage, hysteresis band, snubber characteristics, motor parameters (particularly winding inductance), motor speed, and torque levels. Consequently, managing these fluctuations is quite challenging.
3. Given that the waveforms of the stator magnetic flux are not sinusoidal, *dq* transformation cannot be applied, making accurate control of the magnetic flux unfeasible.

In the DTC method for the BLDC motors, the influence of the magnetic flux difference (F_{st}) on the selection of the voltage vector applied to the inverter is disregarded, focusing solely on the torque difference. As indicated in Table 4, if the actual torque exceeds the hysteresis range, the torque difference (T_{st}) is represented by T_I. Conversely, if the actual torque falls below the hysteresis range, it is denoted by T_D. The DTC method offers several advantages, including rapid response, low torque ripple, a straightforward algorithm, and ease of implementation compared to many contemporary methods.

TABLE. 4. Switching pattern of inverter based on DTC method [15]

F_{ST}	T_{st}	Section					
		θ_1	θ_2	θ_3	θ_4	θ_5	θ_6
F_I	T_I	$V_1(10001)$	$V_2(001001)$	$V_3(011000)$	$V_4(010010)$	$V_5(000110)$	$V_6(100100)$
	T_D	$V_6(100100)$	$V_1(10001)$	$V_2(001001)$	$V_3(011000)$	$V_4(010010)$	$V_5(000110)$
F	T_I	$V_2(001001)$	$V_3(011000)$	$V_4(010010)$	$V_5(000110)$	$V_6(100100)$	$V_1(10001)$
	T_D	$V_5(000110)$	$V_6(100100)$	$V_1(10001)$	$V_2(001001)$	$V_3(011000)$	$V_4(010010)$
F_D	T_I	$V_3(011000)$	$V_4(010010)$	$V_5(000110)$	$V_6(100100)$	$V_1(10001)$	$V_2(001001)$
	T_D	$V_4(010010)$	$V_5(000110)$	$V_6(100100)$	$V_1(10001)$	$V_2(001001)$	$V_3(011000)$

4. ROTOR POSITION IDENTIFICATION SCHEMES

The rotor position identification is crucial in BLDC motors as it directly influences performance, efficiency, and control. Accurate knowledge of the rotor's position enables effective commutation, ensuring smooth operation across varying speeds and loads. Without precise rotor position data, the motor may experience torque fluctuations and inefficiencies, particularly during startup and low-speed conditions. Various methods, including sensor-based techniques like the Hall effect sensors and sensorless approaches, are employed to determine rotor position. Each method has its advantages and limitations, impacting the overall system design. The ability to reliably identify rotor position not only enhances motor responsiveness but also contributes to the longevity and reliability of the motor system, making it a fundamental aspect of the BLDC motor technology in applications ranging from electric vehicles to robotics. Thus, effective rotor position identification is essential for optimizing performance and achieving the desired operational characteristics in the BLDC motors.

4.1. Sensor-Based Methods

Sensor-based methods, as their name implies, are hardware solutions. The sensors commonly used for rotor position detection in the BLDC motors include:

I. Resolvers
II. Hall effect sensors
III. Optical encoders

These three types of sensors differ significantly in terms of cost, operational principles, and applications. In terms of expense, they rank from most to least expensive as follows: resolvers, optical encoders, and the Hall effect sensors. Optical encoders offer high precision and performance but are vulnerable in heavy industrial environments, such as mining and petrochemicals. Their functionality can be compromised by dust or soot, leading to serious operational issues for the BLDC motors. Resolvers provide the highest accuracy for rotor position detection and are suitable for harsh and dusty environments; however, their design and manufacturing costs are substantial, making them advisable only for critical applications. The most commonly used sensor for rotor position detection in the BLDC motors is the Hall effect sensor. While these sensors lack high precision, they are adequate for applications requiring switch state changes every 60 electrical degrees. The following sections will explore the operation of rotary encoders and Hall effect sensors in greater detail.

4.1.1. Resolvers

Resolvers offer the highest accuracy among rotor position sensors and exhibit greater resilience against environmental disturbances compared to other sensor types. They are constructed in various configurations, including reluctance [27], dual-stator [28], single-stator [29], and others. Single-stator resolvers have a main winding called the excitation winding, typically located on the rotor. They also have secondary windings, spaced 90 electrical degrees apart, situated in the stator slots. The excitation voltage of resolvers typically ranges from 1 to 10 kHz. If the resolver rotor has P poles, its accuracy is $P/2$ times that of a two-pole rotary encoder; hence, it is desirable to maximize the number of rotor poles. However, as the resolver speed increases, its accuracy decreases. The resolver transmits the rotor position information to a digital converter. When the motor shaft rotates, sinusoidal voltages are induced in the encoder windings. These sinusoidal input voltages are processed by the digital converter to determine the rotor position. The digital converter block diagram consists of various components, including an excitation circuit, conditioning circuit, sampling block, demodulation block, low-pass filter, and angle tracking block. The conditioning circuit prepares the encoder output for the DSP processing. Demodulation can be performed either software-based within the DSP or hardware-based externally, with the former option reducing manufacturing costs. The excitation voltage waveform may be sinusoidal, square, or pulsed [27-31].

4.1.2. Hall Effect Sensors

Rotary and optical encoder methods offer significantly higher precision compared to Hall effect sensors. In the

BLDC motors, the active switches change every 60 electrical degrees, allowing for the use of slightly less precise methods in non-critical applications. However, determining rotor position using optical or rotary encoders is considerably more expensive than using the Hall effect sensors. By employing just three Hall effect sensors spaced 120 electrical degrees apart, the costs of rotor position detection can be substantially reduced [32], also minimizing the motor's overall size.

Sensorless position detection methods are cost-effective but come with limitations that make the Hall effect sensors preferable. In controlling the BLDC motors, accurately determining both rotor position and actual speed is crucial. The actual rotor speed can often be derived from the rotor position detection system. In the Hall effect sensor-based methods, the time between the activation of two sensors is measured to calculate the rotor's actual speed. Conversely, sensorless methods, particularly those based on back-EMF, experience significant torque and current ripple at low speeds, making accurate speed estimation challenging due to the small back-EMF voltages. Consequently, sensorless approaches may not perform well at low speeds, leading to noisy motor startup. Sensorless methods are also affected by motor parameters, including temperature variations, nonlinear inverter characteristics, and changes in stator winding resistance due to temperature fluctuations, which can disrupt their performance. Therefore, the Hall effect sensors provide a cost-effective means of obtaining rotor position information [33-35].

Typically, three Hall effect sensors are used in the BLDC motors. Each sensor outputs a logical "High" voltage level that lasts for 180 electrical degrees, activating when the north pole of a magnet is near. By analyzing the output signals from these sensors, the switching sequence can be determined. After every 60 electrical degrees, one Hall effect sensor changes state, dividing one electrical cycle into six stages. It is important to note that one electrical cycle does not equate to one full rotor revolution; the number of electrical cycles required for a complete rotation depends on the number of rotor poles [36].

4.2. Sensorless Methods

One of the major drawbacks of sensor-based rotor position detection methods is the difficulty in accurately installing sensors on the motor. This issue is particularly problematic for motors with a high number of poles or compact sizes. Additionally, sensor-based methods increase the overall volume of the motor. These approaches require wired connections between the sensors and the control circuit. Hall effect sensors and optical encoders perform poorly in pumps, high mechanical stress environments, and damp conditions, while rotary encoders can be prohibitively expensive. To address these challenges, sensorless rotor position detection methods can be employed. Sensorless techniques can be broadly categorized into four types:

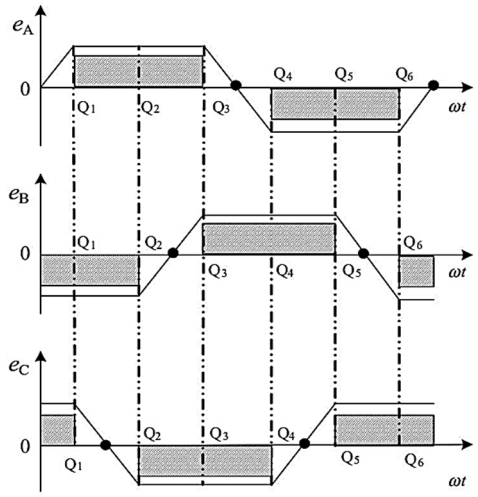

Fig. 14. The relationship between the back-EMF zero-crossing points and the commutation instants [1]

methods based on back-EMF voltage, flux linkage, inductance, and intelligent methods [37,38].

4.2.1. Back-EMF-based Techniques

Back-EMF-based sensorless rotor position estimation methods are among the most widely used techniques currently. These methods identify the zero-crossing points of the back-EMF waveforms and apply a 30-degree delay to generate the commutation signals. Fig. 14 illustrates the relationship between the back-EMF zero-crossing points and the commutation instants. In this figure, e_A, e_B, and e_C represent the back-EMF waveforms, which are 120 electrical degrees apart. Q_1, Q_2, ..., and Q_6 denote the commutation instants. One of the biggest challenges in back-EMF-based methods is the accurate detection of the back-EMF zero-crossing points. The text goes on to discuss some of these methods and their approaches to overcome this challenge [1].

4.2.1.1. Terminal Voltage Measurement Technique

By measuring the voltage at the terminal of the inactive phase, the zero-crossing points of the back EMF can be determined [39]. This can be accomplished through either software or hardware methods; however, this study focuses on the software approach. The mathematical model of the BLDC motor is as follows [1]:

$$\begin{cases} u_{AG} = Ri_A + (L - M)\dfrac{di_A}{dt} + e_A + U_N \\ u_{BG} = Ri_B + (L - M)\dfrac{di_B}{dt} + e_B + U_N \\ u_{CG} = Ri_C + (L - M)\dfrac{di_C}{dt} + e_C + U_N \end{cases} \quad (5)$$

In the aforementioned relation, u_{AG}, u_{BG}, and u_{CG} represent the terminal voltages of the BLDC motor. U_N denotes the neutral point voltage. For the purposes of this analysis, it is assumed that phases A and B are active while phase C is inactive. Under this condition, the relationship between the

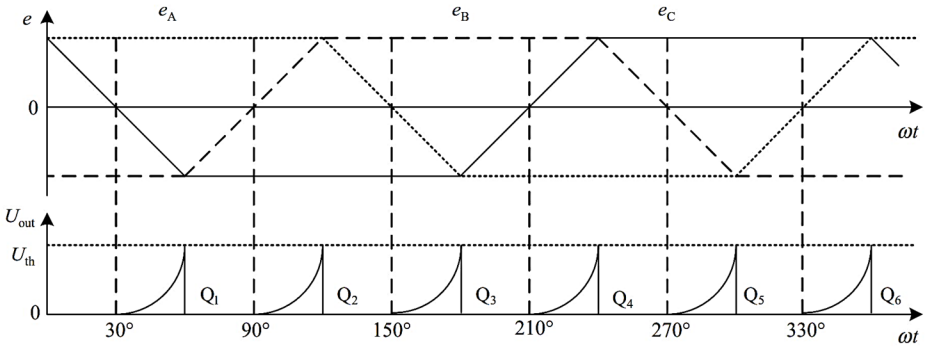

Fig. 15. The relationship between the waveform of the back-EMF voltage integral of the inactive phase and the commutation moments [1]

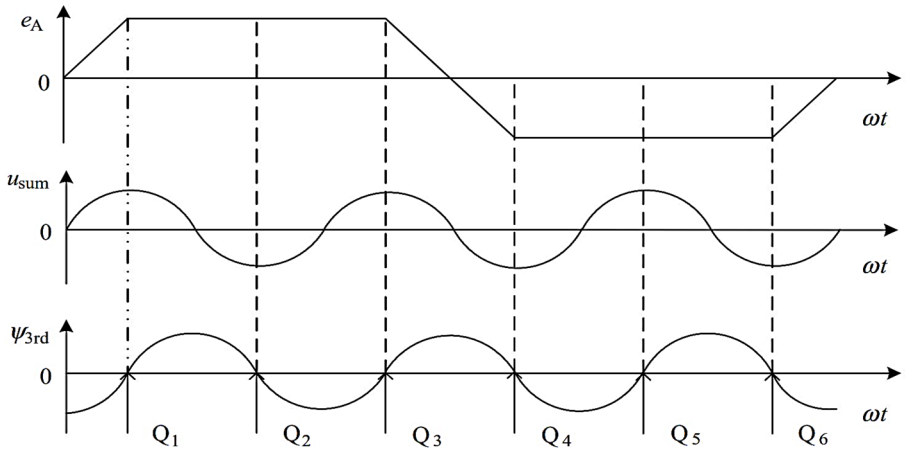

Fig. 16. The phase *a* back-emf, phase voltages summation, and third harmonic of linkage flux [1]

back-EMF and the currents in phases *A* and *B* is expressed as follows [1]:

$$e_A + e_B = 0 \tag{6}$$

$$i_A + i_B = 0 \tag{7}$$

If the terminal voltages of phases *A* and *B* are summed, the following relationship would be obtained:

$$u_{AG} + u_{BG} = R\left(i_A + i_B\right) + \left(L - M\right)\left(\frac{di_A}{dt} + \frac{di_B}{dt}\right) + \left(e_A + e_B\right) + 2U_N \tag{8}$$

Upon substituting (6) and (7) into (8), the following expression for the neutral voltage is derived:

$$U_N = \frac{u_{AG} + u_{BG}}{2} \tag{9}$$

Given that phase *C* is inactive, the back-EMF for phase *C* can be expressed as follows:

$$e_C = u_{CG} - U_N = u_{CG} - \frac{u_{AG} + u_{BG}}{2} \tag{10}$$

Similarly, if phases *A* or *B* are inactive, the following relationships can be derived:

$$e_A = u_{AG} - U_N = u_{AG} - \frac{u_{CG} + u_{BG}}{2} \tag{11}$$

$$e_B = u_{BG} - U_N = u_{BG} - \frac{u_{AG} + u_{CG}}{2} \tag{12}$$

The commutation instants, determined by the electrical angles of the zero-crossing points, exhibit a 30-degree delay. These angles are defined based on the intervals between two preceding zero-crossing points, as follows:

$$\begin{cases} T(k-1) = Z(k-1) + \frac{1}{2}\Delta T \\ \Delta T = Z(k-1) - Z(k-2) \end{cases} \tag{13}$$

In the aforementioned relationship, *T(k-1)* and *Z(k-1)* represent the *(k-1)*th commutation moment and the *(k-1)*th zero-crossing of the back-EMF voltage, respectively. It is important to note that each phase has two zero-crossing points within one cycle. Consequently, these points must be distinguished based on the polarity of the voltage before or after the crossing. Furthermore, the capacitor used prior to the inverter induces a phase shift in the terminal voltage. Therefore, these factors must be considered during software implementation to prevent system malfunctions.

4.2.1.2. Back-EMF Integral Technique

In the back-EMF voltage integral method, the integral of the back-EMF voltage of the inactive phase is

continuously compared with a threshold value [40]. When these two values are equal, it indicates the optimal moment for commutation. Fig. 15 illustrates the relationship between the waveform of the back-EMF voltage integral of the inactive phase and the commutation moments. As shown in Fig. 15, the back-EMF voltage varies approximately linearly, allowing its function to be expressed as follows [1]:

$$e(t) = \pm E_0 t \tag{14}$$

When the back-EMF of the inactive phase crosses the zero point, the integrator must begin to function, as expressed by the following relationship:

In the above equations, E_0, U_{out}, and k represent the slope of the back-EMF waveform, the output voltage of the integrator, and the gain constant of the integrator, respectively.

When the output voltage of the integrator reaches the threshold value U_{th}, the integrator halts, and a commutation signal is generated. The integrator does not initiate operation until the next zero-crossing point of the back-EMF is approached. In the control system, a 30-degree delay is applied to the commutation signals generated from this process. Consequently, the commutation moment for the phase is expressed as follows:

$$U_{out} = \left|\frac{1}{2}\cdot\frac{K_e\omega}{t}\cdot t^2\right| = \left|\frac{1}{2k}K_e\omega t\right| = \left|\frac{1}{2k}\cdot K_e\cdot\frac{\pi}{6}\right| = U_{th} \tag{16}$$

To implement the back-EMF voltage integral method, it is essential to first calculate the threshold value U_{th}. The control system then compares U_{out} and U_{th} in real-time to determine the commutation moment. This approach offers several advantages: it does not require motor speed information, and by adjusting U_{th}, the motor can be advanced or retarded in phase.

4.2.1.3. Back-EMF Third Harmonic Technique

In this method, as the name suggests, the third harmonic of the back-EMF voltage is utilized to determine the optimal commutation moment for the BLDC motor [41,42]. To achieve this, the Fourier transform is applied to the back-EMF voltages of the motor. Subsequently, the components of all fundamental and non-fundamental harmonics are extracted. Thus, the back-EMF voltages can be expressed as follows [1]:

$$\begin{cases} e_A = E_1\sin\theta + E_3\sin3\theta + E_5\sin5\theta + \cdots \\ e_B = E_1\sin\left(\theta - \frac{2\pi}{3}\right) + E_3\sin3\left(\theta - \frac{2\pi}{3}\right) + E_5\sin5\left(\theta - \frac{2\pi}{3}\right) \\ e_C = E_1\sin\left(\theta - \frac{4\pi}{3}\right) + E_3\sin3\left(\theta - \frac{4\pi}{3}\right) + E_5\sin5\left(\theta - \frac{4\pi}{3}\right) \end{cases} \tag{17}$$

In the above equation, θ represents the electrical angle of the rotor. By summing all three equations from (17), the following relationship is obtained:

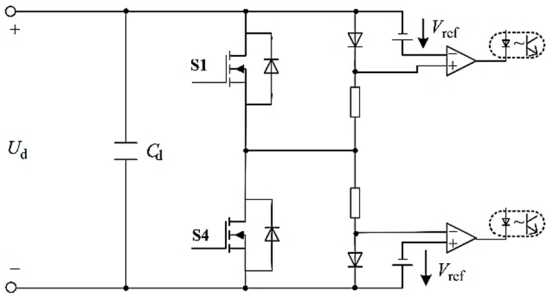

Fig. 17. The commutation instant detection circuit for the freewheeling diode based technique [1]

$$U_{out} = \left|\int_0^t \frac{e(t)}{k}dt\right| = \left|\frac{E_0 t^2}{k}\right| \tag{15}$$

$$\begin{aligned} e_A + e_B + e_C &= 3E_3\sin3\theta + 3E_9\sin9\theta + 3E_{15}\sin15\theta + \cdots \\ &\approx 3E_3\sin3\theta \end{aligned} \tag{16}$$

As mentioned earlier, the phase voltage equations for a BLDC motor are as follows:

$$\begin{cases} u_{AG} = Ri_A + (L-M)\dfrac{di_A}{dt} + e_A \\ u_{BG} = Ri_B + (L-M)\dfrac{di_B}{dt} + e_B \\ u_{CG} = Ri_C + (L-M)\dfrac{di_C}{dt} + e_C \end{cases} \tag{18}$$

It is important to note that the sum of the three-phase currents is equal to zero. Consequently, the following relationship can be derived from the sum of the three-phase voltage equations:

$$\begin{aligned} u_{sum} &= u_A + u_B + u_C \\ &= \left(R + (L-M)\frac{d}{dt}\right)(i_A + i_B + i_C) + (e_A + e_B + e_C) \\ &= e_A + e_B + e_C \approx 3E_3\sin3\theta \end{aligned} \tag{19}$$

The third component of the linkage flux is obtained by integrating (19):

$$\psi_{3rd} = \int u_{sum}dt \tag{20}$$

As shown, (19) encompasses information regarding the third harmonic of the back-EMF voltage. The waveforms of the back-EMF voltage for phase A, the sum of phase voltages, and the third harmonic linkage flux component are depicted in Fig. 16. Notably, the commutation moments coincide precisely with the zero-crossing points of the third harmonic linkage flux curve, eliminating the need for 30 degrees delay. Compared with the terminal voltage measurement methods, the third harmonic voltage approach offers broader speed control capabilities. However, a significant drawback of this method is the high noise levels encountered during low-speed operation.

4.2.1.4. Freewheeling Diode-Based Technique

In the freewheeling diode method, the rotor position is determined based on the conduction state of the

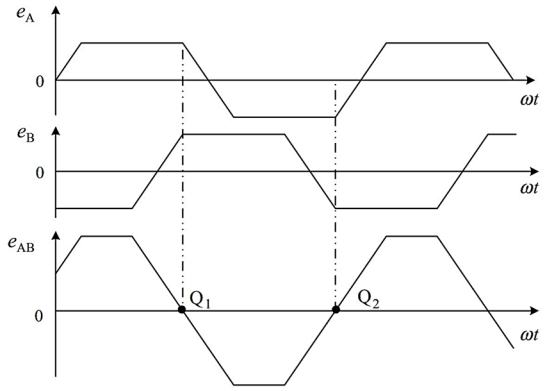

Fig. 18. Comparison of line and phase back-emf waveforms [1]

freewheeling diode. This method is also referred to as the third phase conduction method in some references. To explain the operation of the freewheeling diode method, let's assume that phases *A* and *B* are active while phase *C* is inactive. The PWM-ON switching method is used in this study. In this case, switch S_1 in the upper half-bridge of the inverter operates in PWM mode when phase *C* is inactive, while switch S_6 in the lower half-bridge of phase *B* is continuously on during this interval. When switch S_1 is off, freewheeling diode D_4 is conducting. When switch S_1 is off, the current flows through diode D_4. Therefore, switch S_6 and diode D_4 form the current conduction path. In this case, the terminal voltage of the inactive phase is obtained as follows [1]:

$$u_{CG} = e_C + U_N = e_C + \frac{V_{CE} - V_D}{2} - \frac{e_A + e_B}{2} \quad (21)$$

In the aforementioned relationship, V_{CE} and V_D represent the voltage drop across the power switch and the diode, respectively. For diode D_2 to conduct, the following condition must be satisfied:

$$u_{CG} < -V_D \quad (22)$$

By substituting (21) into (22), the following inequality is derived:

$$e_C - \frac{e_A + e_B}{2} < -\frac{V_{CE} + V_D}{2} \quad (23)$$

When the back EMF of phase *C* crosses the zero point, the (23) would be adjusted as follows:

$$e_C < -\frac{V_{CE} + V_D}{2} \quad (24)$$

The values of V_{CE} and V_D are negligible compared to the back-EMF voltage. The freewheeling diode method enables speed control over a wider range. The commutation instant detection circuit for this method is shown in Fig. 17. The primary drawback of this approach is the requirement of six independent voltage sources in the detection circuit, leading to increased costs.

4.2.1.5. Back-EMF Line Voltage-Based Technique

In many sensor-based rotor position detection methods, a 30-degree delay is applied to the commutation signals after determining the commutation instant. However, using line-to-line back-EMF voltage instead of phase back-EMF eliminates the need for this delay. Moreover, in applications with variable loads, phase voltage-based methods lack sufficient accuracy. This approach utilizes zero-crossing points of line back-EMF voltages to determine the commutation instant, enhancing the precision of the drive and control system. Fig. 18 compares the zero-crossing points of phase and line back-EMF voltages, showing that commutation moments align precisely with the zero-crossings of line back-EMF. Consequently, commutation signals can be derived from the calculations of line back-EMF voltages e_{AB}, e_{BC}, and e_{CA}. The line back-EMF method outperforms phase voltage-based methods at low speeds, and its straightforward implementation is a significant advantage [1, 43].

5. CONCLUSION

This study provided insights into the various drive circuits, control schemes, and rotor position identification methods employed in BLDC motors. The findings highlight the critical role of drive circuits in the effective operation of BLDC motors, directly influencing torque delivery, efficiency, and overall system responsiveness. The well-known drive circuit configurations, including half-wave inverters, split-source half-wave inverters, C-Dump half-wave inverters, and buck-type and buck-boost-type converter-based inverters, emphasizing their respective advantages, disadvantages, and suitability for specific applications, were analyzed. It is evident that the choice of drive circuit configuration is a crucial factor in balancing cost, complexity, and performance. For instance, half-wave inverters, while more compact and cost-effective, are suitable for less sensitive applications due to their reduced efficiency compared to full-wave counterparts. Conversely, split-source half-wave inverters and the C-Dump half-wave inverters offer the ability to operate across all four quadrants of the BLDC motor's performance, making them suitable for applications requiring regenerative braking or reverse operation. Furthermore, the full-wave inverters, including six-switch, H-bridge, and four-switch configurations, are more appropriate for medium and high-power applications. Also, this paper delved into the various control methods employed to manipulate the torque and rotational velocity characteristics of the BLDC motors. These control schemes, such as hysteresis control, the PAM, the PWM, and the DTC, directly impact the switching patterns of the

inverter's power switches, ultimately influencing motor performance.

A critical aspect that has been highlighted in this survey is the importance of accurate rotor position detection for effective commutation and optimal BLDC motor performance. The sensor-based and sensorless approaches have been compared, discussing their respective advantages and limitations. While sensor-based methods provide enhanced accuracy, they come at the expense of increased complexity and cost. Sensorless techniques, on the other hand, offer a more cost-effective solution but may compromise precision under variable load conditions. The appropriate rotor position identification methods must be selected tailored to specific application requirements. The choice between sensor-based and sensorless approaches should be made based on factors such as cost, complexity, and the desired level of precision. In applications where high reliability and performance are paramount, sensor-based methods may be the preferred choice, despite the additional cost and complexity. Conversely, in applications where cost is a critical factor, sensorless techniques may be a viable option, provided that the performance requirements can be met.

REFERENCES

[1] C.-l. Xia, Permanent magnet brushless DC motor drives and controls: *John Wiley & Sons*, 2012.

[2] R. Krishnan, Permanent magnet synchronous and brushless DC motor drives: *CRC Press*, 2017.

[3] S. S. Lee and Y. E. Heng, "Improved Single-Phase Split-Source Inverter with Hybrid Quasi-Sinusoidal and Constant PWM," *IEEE Transactions on Industrial Electronics*, vol. 64, no. 3, pp. 2024-2031, 2017.

[4] D. W. Hart, Power electronics: *Tata McGraw-Hill Education*, 2011.

[5] Chien-Ming Wang and Teng-Jen Chen, "Novel single-stage half-bridge series-resonant buck-boost inverter," *IEEE Transactions on Aerospace and Electronic Systems*, vol. 40, no. 4, pp. 1262-1270, 2004.

[6] Y. Tang, X. Dong, and Y. He, "Active Buck-Boost Inverter," *IEEE Transactions on Industrial Electronics*, vol. 61, no. 9, pp. 4691-4697, 2014.

[7] S. R. Misal, and N. Bhasme, "A review of multi-switch BLDC motor drive," *Innovations in Power and Advanced Computing Technologies (i-PACT)*, Vellore, India, pp. 1-7, 2017.

[8] S. Ray, N. Gupta, R. A. Gupta, "A comprehensive review on cascaded H-bridge inverter-based large-scale grid-connected photovoltaic" *IETE Technical Review*, vol. 34, no. 5, pp. 463-477, 2017.

[9] S. S. Barah and S. Behera, "An Optimize Configuration of H-Bridge Multilevel Inverter," *1st International Conference on Power Electronics and Energy (ICPEE)*, Bhubaneswar, India, 2021.

[10] M. S. Elkerdany, I. M. Safwat, A. M. M. Yossef, and M. M. Elkhatib, "A comparative study on using brushless DC motor six-switch and four-switch inverter for UAV propulsion system," *12th International Conference on Electrical Engineering (ICEENG),* Cairo, Egypt, pp. 58-61, 2020.

[11] V. Krishnakumar, and S. Jeevanandhan, "Four switche three phase inverter control of BLDC motor," *1st International Conference on Electrical Energy Systems*, Chennai, India, pp. 139-144, 2011.

[12] M. E. Zarei, D. Ramírez, C. V. Nicolas, and J. R. Arribas, "Three-phase four-switch converter for SPMS generators based on model predictive current control for wave energy applications," *IEEE Transactions on Power Electronics*, vol. 35, no. 1, pp. 289-302, 2019.

[13] Z. Zeng, C. Zhu, X. Jin, W. Shi, and R. Zhao, "Hybrid space vector modulation strategy for torque ripple minimization in three-phase four-switch inverter-fed PMSM drives," *IEEE Transactions on Industrial Electronics*, vol. 64, no. 3, pp. 2122-2134, 2016.

[14] F. Naseri, E. Farjah, E. Schaltz, K. Lu, and N. Tashakor, "Predictive control of low cost three-phase four-switch inverter-fed drives for brushless DC motor applications," *IEEE Transactions on Circuits and Systems I: Regular Papers*, vol. 68, no. 3, pp. 1308-1318, 2020.

[15] S. Niapour, G. Garjan, M. Shafiei, M. R. Feyzi, S. Danyali, and M. Bahrami Kouhshahi, "Review of permanent-magnet brushless DC motor basic drives based on analysis and simulation study," *International Review of Electrical Engineering*, vol. 9, no. 5, pp. 930-957, 2014.

[16] Q. Li, H. Huang, and B. Yin, "The study of PWM methods in permanent magnet brushless DC motor speed control system," *International Conference on Electrical Machines and Systems*, Wuhan, China, pp. 3897-3900, 2008.

[17] Xiangjun, and C. Boshi, "Influences of PWM mode on the current generated by BEMF of switch-off phase in control system of BLDC motor," *Proceedings of the Fifth International Conference on Electrical Machines and Systems*, Shenyang, China, pp. 579-582, 2001.

[18] M. Uesugi, "Drive control apparatus for brushless DC motor and driving method therefore", *US Patent*, no. 5491393, 1996.

[19] X. Zhang, B. Chen, P. Zhu, and H. Lei, "A new method to minimize the commutation torque ripple in trapezoidal BLDC motor with sensorless drive," *Third International Power Electronics and Motion Control Conference*, Beijing, China, pp. 607-611, 2000.

[20] W. Kun, R. Junjun, T. Fanghua, and Z. Zhongchao, "A novel PWM scheme to eliminate the diode freewheeling in the inactive phase in BLDC motor," *IEEE 35th Annual Power Electronics Specialists Conference*, Aachen, Germany, pp. 2282-2286, 2004.

[21] M. Baszynski, and S. Pirog, "Unipolar modulation for a BLDC motor with simultaneously switching of two transistors with closed-loop control for four-quadrant operation," *IEEE Transactions on Industrial Informatics*, vol. 14, no. 1, pp. 146-155, 2017.

[22] C. Cui, G. Liu, and K. Wang, "A novel drive method for high-speed brushless DC motor operating in a wide range," *IEEE Transactions on power electronics*, vol. 30, no. 9, pp. 4998-5008, 2014.

[23] Y.-S. Lai, K.-Y. Lee, J.-H. Tseng, Y.-C. Chen, and T.-L. Hsiao, "Efficiency comparison of PWM-controlled and PAM-controlled sensorless BLDCM drives for refrigerator applications," *IEEE Industry Applications Annual Meeting*, New Orleans, LA, USA, pp. 268-273, 2007.

[24] K.-H. Kim, and M.-J. Youn, "Performance comparison of PWM inverter and variable DC link inverter schemes for high-speed sensorless control of BLDC motor," *Electronics Letters*, vol. 38, no. 21, pp. 1-2, 2002.

[25] S. B. Ozturk, W. C. Alexander and H. A. Toliyat, "Direct Torque Control of Four-Switch Brushless DC Motor With Non-Sinusoidal Back EMF," *IEEE Transactions on Power Electronics*, vol. 25, no. 2, pp. 263-271, 2010.

[26] A. Khazaee, H. A. Zarchi, G. A. Markadeh and H. Mosaddegh Hesar, "MTPA Strategy for Direct Torque Control of Brushless DC Motor Drive," *IEEE Transactions on Industrial Electronics*, vol. 68, no. 8, pp. 6692-6700, 2021.

[27] L. Sun, "Analysis and improvement on the structure of variable reluctance resolvers," *IEEE Transactions on Magnetics*, vol. 44, no. 8, pp. 2002-2008, 2008.

[28] S. Hajmohammadi, H. Saneie, Z. Nasiri-Gheidari, and F. Tootoonchian, "Optimal design and performance analysis of a double-sided multiturn wound-rotor resolver," *IEEE/ASME Transactions on Mechatronics*, vol. 27, no. 1, pp. 493-500, 2021.

[29] B. Rahrovi, "A Review and Comparison of the DSP-Based Resolver to Digital Conversion Methods," *IEEE Texas Power and Energy Conference (TPEC)*, College Station, TX, USA, pp. 1-6, 2019.
[30] S. C. M. Reddy, and K. N. Raju, "Inverse tangent based resolver to digital converter A software approach," *International Journal of Advances in Engineering & Technology*, vol. 4, no. 2, pp. 228, 2012.
[31] J.-D. Sun, G.-Z. Cao, S.-D. Huang, and H. Qiu, "Software-based resolver-to-digital converter using the PLL tracking algorithm," *13th International Conference on Ubiquitous Robots and Ambient Intelligence (URAI)*, Xian, China, pp. 719-723, 2016.
[32] H. Mehta, V. Joshi, U. Thakar, M. Kuber and P. Kurulkar, "Speed control of PMSM with Hall sensors using DSP TMS320F2812," *IEEE 11th International Conference on Power Electronics and Drive Systems*, Sydney, NSW, Australia, pp. 295-300, 2015.
[33] G. Liu, B. Chen, and X. Song, "High-precision speed and position estimation based on Hall vector frequency tracking for PMSM with bipolar Hall-effect sensors," *IEEE Sensors Journal*, vol. 19, no. 6, pp. 2347-2355, 2018.
[34] Y.-P. Yang, and Y.-Y. Ting, "Improved angular displacement estimation based on Hall-effect sensors for driving a brushless permanent-magnet motor," *IEEE Transactions on Industrial Electronics*, vol. 61, no. 1, pp. 504-511, 2013.
[35] Y. Liu, J. Zhao, M. Xia, and H. Luo, "Model reference adaptive control-based speed control of brushless DC motors with low-resolution Hall-effect sensors," *IEEE Transactions on Power Electronics*, vol. 29, no. 3, pp. 1514-1522, 2013.
[36] A. Sathyan, "Digital PWM Control of Brushless DC Motor Drives," Illinois Institute of Technology, Chicago, IL, 2008.
[37] S. Wang, and A.-C. Lee, "A 12-step sensorless drive for brushless DC motors based on back-EMF differences," *IEEE Transactions on Energy Conversion*, vol. 30, no. 2, pp. 646-654, 2014.
[38] S. Chen, G. Liu, and L. Zhu, "Sensorless startup strategy for a 315-kW high-speed brushless DC motor with small inductance and non-ideal back EMF," *IEEE Transactions on Industrial Electronics*, vol. 66, no. 3, pp. 1703-1714, 2018.
[39] T. Kim, Chungil Kim, and J. Lyou, "A new sensorless drive scheme for a BLDC motor based on the terminal voltage difference," *37th Annual Conference of the IEEE Industrial Electronics Society*, Melbourne, VIC, Australia, pp. 1710-1715, 2011.
[40] H. Jin, G. Liu, and S. Zheng, "Commutation Error Closed-Loop Correction Method for Sensorless BLDC Motor Using Hardware-Based Floating Phase Back-EMF Integration," *IEEE Transactions on Industrial Informatics*, vol. 18, no. 6, pp. 3978-3986, 2022.
[41] X. Song, B. Han, and K. Wang, "Sensorless Drive of High-Speed BLDC Motors Based on Virtual Third-Harmonic Back EMF and High-Precision Compensation," *IEEE Transactions on Power Electronics*, vol. 34, no. 9, pp. 8787-8796, 2019.
[42] X. Song, B. Han, S. Zheng and J. Fang, "High-Precision Sensorless Drive for High-Speed BLDC Motors Based on the Virtual Third Harmonic Back-EMF," *IEEE Transactions on Power Electronics*, vol. 33, no. 2, pp. 1528-1540, 2018.
[43] G. Liu, C. Cui, K. Wang, B. Han, and S. Zheng, "Sensorless Control for High-Speed Brushless DC Motor Based on the Line-to-Line Back EMF," *IEEE Transactions on Power Electronics*, vol. 31, no. 7, pp. 4669-4683, 2016.